

AD-A076 103

NEW YORK UNIV N Y DEPT OF PHYSICS

F/G 20/5

PHOTON ECHOES IN STANDING WAVE FIELDS: TIME SEPARATION OF SPATI--ETC(U)

SEP 79 J LE GOUET , P R BERMAN

N00014-77-C-0553

UNCLASSIFIED

NL

1 of 1
AD
A076103



END
DATE
FILMED
12-74
DDC

6 Photon echoes in standing wave fields;
time separation of spatial harmonics,

12

LEVEL II

AD A 0761 03

10 J.-L. LE GOUET

Laboratoire Aimé Cotton, C.N.R.S. II, Pât. 505, 91405-Orsay, France,

and

P. R. BERMAN

Physics Department, New York University, 4, Washington Place,

New York, N. Y. 10003, U. S. A.

Reproduction in whole or in part is permitted for any purpose of the United States Government.

Supported by the U.S. Office of Naval Research under Contract No. N00014-77-C-0553

DDC
RECEIVED
NOV 2 1979
B

11 September 1979

12/18

Abstract :

A calculation is presented to describe the response of an atomic system subjected to two strong standing wave field pulses separated in time. One finds a sequence of output pulses following the input ones, reminiscent of classical photon echoes. A physical picture of the processes involved in echo formation is presented and connection is made with the classical picture of photon echoes. The application of these techniques to collision studies is emphasized. It is shown that studies of echoes produced by standing wave fields can prove advantageous for exploring the effects of small angle scattering on both level populations and atomic coherences.

DDC FILE COPY

DISTRIBUTION STATEMENT A
Approved for public release;
Distribution Unlimited

THIS DOCUMENT IS BEST QUALITY PRACTICABLE
THE COPY FURNISHED TO DDC CONTAINED A
SIGNIFICANT NUMBER OF PAGES WHICH DO NOT
REPRODUCE LEGIBLY.

79 09 17 078

406 850

B

I. Introduction.

There has been recent interest in using time resolved methods in laser spectroscopy. These include time resolved saturation spectroscopy¹, free-induction decay², photon echo^{3,4}, quantum beats⁵, coherent Raman beats⁶, superradiance⁷, and excitation in separated fields⁸⁻¹³. In most of these experiments one observes the transient response of atoms to the application or removal of laser fields. In addition to providing a means for carrying out high precision spectroscopy, these methods are useful, to varying degrees, for studying relaxation processes.

In this paper we consider the response of an atomic system to excitation by separated fields, sometimes referred to as optical Ramsey fringes. To observe optical Ramsey fringes, one applies a laser-generated standing wave to atoms during a short time τ , at two instants separated by a delay T . Experimentally, this process has been studied using gas cells¹⁰⁻¹³ as well as atomic beams^{8,9} for both two-photon^{10,12} and one-photon^{8,9,11,13} excitation. In the case of two-photon transitions, which are free from the Doppler effect, the evolution of the atoms after the second pulse is probed by the fluorescence decay from the upper level. For one-photon transitions, the field-induced coherence among the atomic dipoles is rapidly destroyed for different velocity subclasses of atoms owing to the Doppler effect, except at a time T after the second pulse. At this instant a coherent radiation is emitted by the gas, which is reminiscent of the classical photon echo. In either case the signals exhibit a detuning-dependent structure of width $1/T$, which does not exist in the usual photon echo. The ultimate resolution of separated field spectroscopy (with width $(T)^{-1}$) may be much better than that in saturation spectroscopy (limited by transit-time broadening).

In the last papers of the Group of Novosibirsk,¹¹⁻¹³ a new feature was noticed, which is the occurrence of coherent radiations, not only at time T , but also at $2T$, $3T$ after the second pulse. The aim of this article is to qualitatively and quantitatively discuss the origin of the successive coherent radiation in separated fields (C R S F). The build up of echoes at successive times is directly connected with the cancellation of the Doppler phase of various spatial harmonics of both the atomic coherences and level-populations. We show that the spatial component of order n between the two pulses, is the source of an echo at time nT after the second pulse. The characteristics of the phenomenon in the frequency domain are investigated and the difference with the usual photon echo is elucidated. Moreover a calculation of the C R S F intensity is carried out using a simple model.

In Sect. II, the C R S F intensity is calculated, assuming that the field seen by the atoms is provided by the external fields only (i. e. polarization fields are neglected). The details of this calculation are given in Appendix A. Discussions of the origin of the various echoes and the detuning dependence of the fields is given in Sect. III and IV, respectively. Finally, the possibilities of using C R S F for collisional studies is explored in Sect. V.

| | |
|----------------------------|---|
| ACCESSION for | White Section <input checked="" type="checkbox"/> |
| NTIS | Buff Section <input type="checkbox"/> |
| DDC | UNANNOUNCED <input type="checkbox"/> |
| JUSTIFICATION | PER LETTER |
| BY | DISTRIBUTION/AVAILABILITY CODES |
| Dist. AVAIL and/or SPECIAL | A |

II. C R S F Intensity.

Consider a gas cell (Fig. 1) illuminated by two successive standing wave laser pulses. The pulses are applied at times t_0 and t_1 having durations τ_0 and τ_1 respectively. The laser field of frequency ω is taken to be of the form:

$$\vec{E}(z,t) = \mathbf{i} E_0 \cos \omega t \sin kz [\theta(t_0) + \theta(t_1)]$$

where $\theta(t_i) = \begin{cases} 0 < (t-t_i) < \tau_i \\ 0 \text{ otherwise} \end{cases}$, and \mathbf{i} is a unit vector in the direction of polarization.

In the rotating wave approximation, the equations of motion for density matrix elements $\rho(z, v_z, t)$ (only motion in the direction of the field propagation vector need be considered) are:

$$\begin{aligned} \frac{\partial \rho_{11}}{\partial t} + v_z \frac{\partial \rho_{11}}{\partial z} &= \mathbf{i} \chi (\rho_{21} e^{-i\omega t} - \rho_{12} e^{i\omega t}) \sin kz [\theta(t_0) + \theta(t_1)] - \gamma_{11} \rho_{11} \\ \frac{\partial \rho_{22}}{\partial t} + v_z \frac{\partial \rho_{22}}{\partial z} &= \mathbf{i} \chi (\rho_{12} e^{i\omega t} - \rho_{21} e^{-i\omega t}) \sin kz [\theta(t_0) + \theta(t_1)] - \gamma_{22} \rho_{22} \\ \frac{\partial \rho_{12}}{\partial t} + v_z \frac{\partial \rho_{12}}{\partial z} &= \mathbf{i} \chi (\rho_{22} - \rho_{11}) e^{-i\omega t} \sin kz [\theta(t_0) + \theta(t_1)] - \gamma_{12} \rho_{12} - i\omega_0 \rho \end{aligned} \quad (1)$$

where ω_0 is 1-2 transition frequency, $\chi = \mu E_0 / 2\hbar$, μ is the dipole moment associated with the transition 1-2 and γ_{ij} is the natural decay rate of ρ_{ij} .

It is assumed that the applied pulses are well separated ($t_1 - t_0 \gg \tau_k$), and that the detuning $\Delta = \omega - \omega_0$, and decay rates γ_{ij} satisfy $|\Delta| \tau_k \ll 1$, $\gamma_{ij} \tau_k \ll 1$, respectively, as is common experimentally. Moreover, to insure that the Doppler dephasing between pulses is complete, one assumes that $ku T \gg 1$, where u is the

width of the thermal velocity distribution. Finally, the effect of the polarization fields on the atoms is neglected, which is valid provided that the echo fields are much less intense than the external ones. In these limits Eqs. 1 are solved in Appendix A.

All spatial harmonics are contained in the atomic polarization $P = \mu(\rho_{12} + \rho_{21})$ which is of the form:

$$(2) \quad P(v_z, z, t) = P_c(v_z, z, t) \cos \omega_0 t + P_s(v_z, z, t) \sin \omega_0 t$$

where P_c and P_s are slowly varying functions of time, compared with $\cos \omega t$. However, it follows from this form of the polarization and Maxwell's equations that only the component of $P(v_z, z, t)$ proportional to $\sin kz$ gives rise to a significant electric field (i. e. the absence of polarization frequencies $2\omega_0, 5\omega_0, \dots$ implies that polarization components varying as $\sin 3kz, \sin 5kz, \dots$ are negligible). Thus it suffices to consider:

$$(3) \quad \bar{P}(v_z, z, t) = \frac{2k}{\pi} \int_{-\pi/k}^{\pi/k} \sin k(z-z') P(v_z, z', t) dz'$$

where $\bar{P}(v_z, z, t)$ is now a slowly varying function of z compared with $\sin kz$. The echo field is then determined from Maxwell's Eqs. as:

$$(4) \quad \bar{E}(v_z, z, t) = 2ikf [\bar{P}_c(v_z, z, t) \sin \omega_0 t + \bar{P}_s(v_z, z, t) \cos \omega_0 t] \sin kz$$

where:

$$(5) \quad \bar{P}_c(v_z, z, t) = 2v_z/k \int_0^{\pi/k} P_c(v_z, z', t) \sin k(z-z') dz'$$

and l is the length of the sample. The echo amplitude given by:

$$(6) \quad \mathcal{E}(z,t) = \int 2kx \left[\bar{E}_0(v_z, z, t)^2 + \bar{E}_0(v_z, z, t) \right]^{1/2} dv_z$$

is calculated in Appendix A (using the simplifying, but not critical,

assumption that $Y_{11} = Y_{22} = Y$) as:

$$(7) \quad \mathcal{E}(z,t) = 4kx \int dv_z N_0(v_z, z, t_0) \left[A e^{-Y_{12}^2} \cos \Delta t + B e^{-Y^2} \right]$$

where

$$N_0(v_z, z, t_0) = \rho_{22}(v_z, z, t_0) - \rho_{11}(v_z, z, t_0)$$

is the population difference density at $t=t_0$, just before the first pulse, and

$$(8) \quad A = \sum_{\text{odd } n} \left[\frac{4x}{kv_z} \sin\left(\frac{kv_z \tau_1}{2}\right) \right] \times J_n \left[\frac{4x}{kv_z} \sin\left(\frac{kv_z \tau_0}{2}\right) \right]$$

$$B = \sum_{\text{even } n} \left[\frac{4x}{kv_z} \sin\left(\frac{kv_z \tau_1}{2}\right) \right] \times \exp[-Y_{12}(z-t)] \times \cos [kv_z(n\tau - (t-t_0))]$$

The physical content of this equation will be discussed in the next two sections. We may note here some general features of the solution. The echo amplitude is a maximum for $t-t_1 = n\tau$ ($n = \text{integer}$). For other times, the velocity integration leads to a negligible echo amplitude. The maximum amplitude of the n th echo is given by:

$$(9) \quad \mathcal{E}_{\text{max}}(z, t + n\tau) = (-1)^n 4kx \int dv_z N_0(v_z, z, t_0) \times J_{n+1} \left[\frac{4x}{kv_z} \sin\left(\frac{kv_z \tau_1}{2}\right) \right] J_n \left[\frac{4x}{kv_z} \sin\left(\frac{kv_z \tau_0}{2}\right) \right] e^{-Y_{12}^2 n \tau} \times \begin{cases} e^{-Y^2} & n \text{ odd} \\ e^{-Y^2} & n \text{ even} \end{cases} \cos \Delta t$$

For odd n the maximum amplitude oscillates as a function of detuning Δ , with the fringes having a width $\sim 1/\tau$. For even n , the signals do not exhibit this detuning dependence. From Eqs. 7, 8, one can see that the duration of a given echo in time is $[k\Delta v_z]^{-1}$ where Δv_z is the range of significant v_z entering the integration in Eq. (7); the range Δv_z is a function of x, kv_z, τ_0, τ_1 . The general qualitative features of the results are illustrated schematically in Fig. 2.

One can determine the most suitable values of parameters τ_0, τ_1, x in order to maximize the intensity of a given echo. As a first attempt of this choice of parameters, consider the simple situation where all the velocity classes are equally excited by the pulses, i. e. $kv_z \ll 1$. In this limit the arguments of the Bessel functions reduce to $2x\tau_0$ and $2x\tau_1$ respectively. Taking a Maxwellian distribution for N_0 :

$$N_0(v_z) = (N_0/\sqrt{\pi}) \exp(-v_z^2/u^2)$$

one obtains the echo:

$$(10) \quad \mathcal{E}(t) = 4kx N_0 e^{-\frac{k^2 u^2}{4}(n\tau - (t-t_1))^2} [A' e^{-Y_{12}^2} \cos(\Delta t) + B' e^{-Y^2}]$$

where

$$(11) \quad \begin{aligned} A' &= \sum_{n \text{ odd}} (-1)^n J_{n+1}(2x\tau_1) J_n(2x\tau_0) \times \exp[-Y_{12}(t-t_1)] \\ B' &= \sum_{n \text{ even}} J_{n+1}(2x\tau_1) J_n(2x\tau_0) \times \exp[-Y_{12}(t-t_1)] \end{aligned}$$

The duration of each of these echoes (at half maximum) is $3.4/ku$, and to maximize $\mathcal{E}(t), \tau_0$ and τ_1 must be chosen so that the Bessel functions of the observed echo have their first maximum for $2x\tau_0$ and $2x\tau_1$:

$$X \tau_0 = .9 \text{ and } \tau_1 = 1.72 \tau_0 \text{ for } n=1$$

$$X \tau_0 = 1.55 \text{ and } \tau_1 = 1.35 \tau_0 \text{ for } n=2$$

In the limit $ku \ll 1$ under consideration, this optimization procedure requires field strengths $X \gg ku$.

The ratio R_n of the optimized intensity of the first echo to that of the others is shown on Tab. 1.

| n | 1 | 2 | 3 | 4 | 5 |
|-------|---|------|-----|------|---|
| R_n | 1 | 1.82 | 2.7 | 3.57 | 5 |

Table 1

If $ku \gg 1$, Eq. 7 must be evaluated by a numerical integration. Figures 3 and 4 show ρ_{\max} for the two first echoes, as a function of $ku \tau_1$ for several values of X . In this calculation the ratio between τ_0 and τ_1 is fixed at the optimum value which has been determined previously for the limiting case $ku \tau \ll 1$. It turns out that the intensity maxima shown by Fig. 3 and 4 are approximately located at the same values of $X \tau_0$ and $X \tau_1$, as in the $ku \tau_1 \ll 1$ case. The echo amplitude maximum is decreased by a factor 2 (first echo) or a factor 2.8 (second echo) when the Rabi frequency is changed from $2ku$ to $.2ku$.

Figures 5 and 6 represent the time evolution of the echoes around the instant $t_1 + nT$. For each value of X , τ_0 and τ_1 are chosen to give the maximum intensity. The duration of the echoes (at half maximum) is increased from about $3.5/ku$ to $8/ku$ (first echo) and

$3.5/ku$ to $12/ku$ (second echo) when X varies from $2ku$ to $.2ku$. The physical implications of the above results are discussed in the next two sections.

III. Physics of echo formation.

To investigate the physical origin of the echoes, we first consider the limiting case $ku \tau \ll 1$ (all velocity subclasses excited by the pulses). For an initial given phase kz of the applied field at (z, t_0) , the phase of the m -order spatial harmonic of the induced polarization is $m k z$ (m odd). From time t_0 to t with the field off, the atoms keep the same phase $m k z$. Owing to their motion the atoms at (z, t) are the ones which were at $(z_0 = z - v_z(t-t_0), t_0)$. Consequently the spatial phase of atoms with velocity v_z at z is:

$$\rho_m(v_z, z, t) = m k z_0 = m k z - m k v_z(t-t_0)$$

In a standing wave field, populations as well as off-diagonal density matrix elements acquire phases. Thus the phase of an arbitrary density matrix element harmonic at $t = t_1$, is $m k z - m k v_z(t_1-t_0)$ where n can be even (population) or odd (polarization). The second pulse causes each n th harmonic, present at time t , to drive the m th harmonic of the polarization. The phase of the m th harmonic after the pulse is obtained by adding $(m-n)kz$ to the phase of the n th harmonic before the pulse. This leads to:

$$\rho_m(v_z, z, t_1) = m k z - m k v_z(t_1-t_0)$$

is either a population or a polarization component depending on whether n is even or odd, coherent radiation in separated fields is an extension of photon echo in traveling wave fields, where only the lowest polarization components may be excited. The usual interpretation of photon echo in gases considers the effect of the second pulse as a reversal of the Doppler phase⁴:

$$-kv(t_1 - t_0) \rightarrow kv(t_1 - t_0).$$

This result is a limiting case of the more general result in C R S F where the second pulse induces a change of $(1-n)kv(t_1 - t_0)$ in the Doppler phase (for classical photon echo $n = -1$). Thus the presence of the various echoes may be explained by the simple "phase-jump" picture.

The time duration of C R S F may also be explained using a simple picture. The atomic dipoles lose their relative phase coherence in a time equal to the inverse of the frequency bandwidth excited by the laser fields. If $ku \tau_1 \ll 1$, all velocity subclasses are equally excited by the field, giving an excitation bandwidth of ku and consequently, an echo duration of $(ku)^{-1}$. For larger values of $ku \tau_1$ such that $ku \tau_1 \gg 1$, the excitation bandwidth approaches τ_1^{-1} , leading to an echo duration $\sim (\tau_0 + \tau_1)$. This effect is clearly seen in Figs. 5 and 6 as the echo duration increases with $ku \tau_1$.

Excitation bandwidth is also an important factor in explaining the decrease in echo amplitude with decreasing field strength shown in Figs. 5 and 6. For large field strengths leading to optimization pulse widths such that $ku \tau_1 \ll 1$, all velocity subclasses are equally excited and the parameters λ , τ_0 , τ_1 can be chosen to

this total phase differs from the value of φ_m before the pulse by a phase jump $(m-n)kv_2(t-t_0)$. Note that the phase of the m th harmonic after the pulse actually reflects the time development of the n th harmonic, and not that of the m th harmonic, between t_0 and t_1 . In the same way that the phase at time t after the first pulse was obtained, one can calculate the spatial phase at time $t > t_1$, as:

$$\varphi_m(v_2, z, t) = m k z - kv_2(n(t-t_1) + nT) \quad \text{where } T = t_1 - t_0.$$

All the velocity-classes of the polarization combine their contributions to produce coherent radiation of the gas after the second pulse. The spatial average gives rise to negligible contributions from the various harmonics (provided the dimension of the sample is much larger than the radiation wave length) except for the components having spatial phase $\pm k z$. Thus, the signal originates from components such that $m = \pm 1$, with a phase:

$$\varphi_{\pm 1}(v_2, z, t) = \pm k z - kv_2(nT \pm (t-t_1)).$$

In the integration over v_2 , the atomic polarization is small, owing to the Doppler phase $kv_2(nT \pm (t-t_1))$, except at times $t = t_1 + |n|T$ when this Doppler phase is zero. Thus an echo occurs at time $|n|T$ after the second pulse and reflects the build-up of either polarization (n odd) or population (n even) harmonics in the $t_0 \rightarrow t_1$ region. Figure 7 represents this result for the case $n = +8$, $m = -1$, $s = 0$. The result is analogous to that in classical photon echoes— independent of velocity, all dipoles are in phase at a specific time where an echo is observed. Since the n th harmonic

to maximize each echo intensity independently of velocity [see Eq. (9) in which the Bessel function arguments are velocity independent for $ku \tau_1 \ll 1$]. As the field strength decreases, the optimal pulse widths are such that $ku \tau_1 \gg 1$. The condition $ku \tau_1 > 1$ corresponds to atoms moving through at least one wavelength of the standing wave field pattern during the pulses. Each atom starting at (z_0, t_0) then experiences an average field (see Appendix B)

$$\langle \psi(z_0, t_0) \rangle_{t_0, t_0 + \tau} = \frac{2\gamma}{kv_z \tau} \sin(kz_0 + \frac{kv_z \tau}{2}) \sin(\frac{kv_z \tau}{2})$$

which is velocity dependent if $ku \tau \gg 1$. Thus a set of parameters which is optimal for one velocity subclass is not optimal for another [see Eq. (9) in which the Bessel function arguments depend on v_z if $ku \tau \gg 1$]. One is effectively using fewer atoms to provide the echo signal (atoms having $kv_z \tau_1 < 1$ are most efficient) as $ku \tau$ increases, leading to a decrease in echo amplitude.

IV. Detuning dependence.

Following the first pulse, the induced atomic polarization oscillates freely at frequency ω_0 while the level populations exhibit no oscillatory behaviour [see Eqs. (1) for ρ_{12} and ρ_{11} , respectively]. When the second pulse acts on the system (assuming that both pulses arise from the same CW laser) the atomic dipoles have acquired a temporal phase difference Δt with the field. For C R S F echoes driven by

polarization harmonics (odd n), the echo amplitudes are maximal if this phase difference is an integral multiple of 2π and they oscillate as a function of Δ with period π giving rise to "fringes" of width $1/\tau$. For C R S F echoes driven by population harmonics (even n), the phase difference plays no role and no fringes appear.

The structure is typical of Ramsey fringes in which one creates a polarization phase difference by sampling a field at two separate times. This effect is also present in traveling wave photon echoes, but in a less useful way. For traveling wave fields, the detuning always enters as $\Delta - \vec{k} \cdot \vec{v}$ so that, in order to achieve the Doppler phase cancellation necessary for echo formation, the detuning dependence as well as the Doppler phase, vanishes at $t = 2T$. The traveling wave echo exhibits a detuning dependence of $\cos \Delta(t - 2T)$ which, for $t = 2T \pm$ (time duration of the echo), gives a fringe pattern of width $\sim 1 / (\text{echo duration}) \gg \tau^{-1}$. Thus C R S F is much better suited for high precision spectroscopy than traveling wave photon echoes.

The fringe pattern in C R S F extends for a range of detuning $|\Delta| \tau \lesssim 1$, after which it disappears. This result is in contrast to typical Ramsey fringe patterns where only the central fringe may be seen (the other fringes are lost owing to phase destruction arising from different values of v for different velocity groups).

V. Collisions.

C R S F offers some interesting possibilities for collisional studies. Echo formation is intimately related to the spatial phases acquired by atoms as a result of their motion following application of the field. An echo corresponds to the rephasing of the signal at some particular instant $t = t_1 + nT$ when the atoms of velocity v_z are at distance nTv_z from their position at the time of the second pulse (see Fig. 7). Collisions during the time of flight, which prevent the atoms of a given v_z from being at the right position at the right time, result in a decrease of the echo intensity. This phenomenon of "Collisional Doppler dephasing" was already observed in photo-echo experiments.⁴ In that case the signal reflects only the evolution of the first spatial harmonic of the atomic coherence. In C R S F, the spatial harmonics of the population difference, as well as coherences, contribute to the echo formation. Thus the C R S F method extends the possibility of observing a "Collisional Doppler dephasing effect" to the population difference. Moreover, the spatial structure may be probed systematically since every spatial harmonic produces a C R S F echo. However, the relative contribution of an harmonic decreases with increasing n since the detected atoms have a phase associated with the n harmonic during the time between the two pulses only and this delay is smaller and smaller in comparison with the total time of flight $(n+1)T$ as n increases. Therefore most of the interest of the method seems to be concentrated in the first few echoes.

It is true that the observed microscopic collisional process - namely the velocity-changing process - is the same one which can be

investigated in steady state saturation spectroscopy (S S S). However in S S S the contribution of the coherence and of the level population are mixed in the same signal. This may present difficulties of interpretation when coherence and level populations are both sensitive to the velocity changing effect. In contrast in C R S F the occurrence of distinct echoes enables one to separate the coherence and the level population signals.

In order to illustrate the physics involved in collisional Doppler dephasing, we adopt a simple model with the following features:

- (1) binary, foreign gas collisions in the impact approximation, (2) equal natural decay and inelastic collisional rates for levels 1 and 2,¹⁶ (3) inelastic collisions that can be accounted for by one rate constant Γ_1 for all density matrix elements,⁽⁴⁾ short-pulse times $ka \tau \ll 1$ such that all velocity subclasses are equally excited¹⁷. With these assumptions we need consider only elastic collisions and do so using three collision models¹⁸.

(A) - In the first model, collisions are assumed to produce only instantaneous phase changes on atomic coherences. This model is valid generally for electronic and vibrational transitions.¹⁹ For echoes driven by coherences, the effect of collisions is to replace γ_{12} by a collision broadened Γ_{12} and Δ by a collisionally shifted Δ' giving a maximum echo amplitude

$$\begin{aligned} \cdot \int_{-\infty}^{\infty} \max(t_1+nT) = (-)^n \times 4\pi kL \int dv_z N_0(v_z, t_0) \\ \times J_{n+1}(2k\tau_0) J_n(2k\tau_1) e^{-\Gamma_1(1+n)T} \cdot x \cdot e^{-\Gamma_{12}(1+n)T} \cos \Delta' T \end{aligned} \quad (12)$$

exp(i n kv_z dt - i \int_{t_0}^{(n+1)T} kv_z dt) over collisions, and given by 4, 19

$$\begin{aligned} \mathcal{E}_{\max}^2(t_1 + nT) &= (-1)^n 4\pi kL \int dv_z N_0(v_z, z, t_0) \\ &\times J_{n+1}(2\chi \tau_0) J_n(2\chi \tau_1) e^{-\Gamma_1(1+n)T} \gamma_{12}^{-n} T \\ (14) \quad &\times \left\{ \frac{1 - (-1)^n}{2} \cos \Delta T e^{-\gamma_{12} T} + \frac{1 + (-1)^n}{2} e^{-\gamma T} \right\} \\ &\times \begin{cases} \exp(-\alpha \Gamma (nk\Delta u)^2 \tau^2 (1+n)) & nk\Delta u T \ll 1 \\ \exp(-\Gamma (1+n)T) & nk\Delta u T \gg 1 \end{cases} \end{aligned}$$

where n is even or odd.

(C) - A modified collision model, valid for collision interactions that are nearly state independent allows for both a velocity change and small phase shift to occur in level coherences as a result of a collision. This model, which may be valid for some vibrational transitions, can be described by replacing γ_{12} and Δ appearing in Eq. (14) by collisionally modified values Γ_{12} and Δ' . It should be noted that even small collisional shifts may be important in high precision spectroscopy.

An examination of Eqs. (13) and (14) reveals the special functional dependence on T in the factor which comes from velocity changes in small angle scattering. Thus C R S F could be very useful to extract this latter effect from the background of other collisional contributions (inelastic collisions, phase interrupting collisions, strong collisions). Photon echo in traveling waves has already proved useful for that purpose⁴ but, as it has been said previously, coherences only may be probed using classical photon echoes, while C R S F allows a study of collisional effects on level populations as well. The same possibility

For echoes driven by populations, the Doppler phase factor $\exp \int_0^T i n kv_z dt$ developed between t_0 and t_1 by the nth harmonic (n even), must be averaged over velocity changing collisions. Following Ref. 4, one can obtain:

$$\begin{aligned} \mathcal{E}_{\max}^2(t_1 + nT) &= (-1)^n 4\pi kL \int dv_z N_0(v_z, z, t_0) \\ &\times J_{n+1}(2\chi \tau_0) \times J_n(2\chi \tau_1) e^{-\Gamma_1(1+n)T} \\ (13) \quad &\times \begin{cases} e^{-\gamma T} \times e^{-\Gamma_{12} T} & nk\Delta u T \ll 1 \\ e^{-\alpha \Gamma (nk\Delta u)^2 \tau^2} & nk\Delta u T \gg 1 \end{cases} \end{aligned}$$

where Γ is the elastic collision rate, Δu is the rms change in velocity per collision and α is a constant of order unity which depends on the specific collision kernel describing the collisions.¹⁹ Thus, one can probe elastic velocity changing collisions with this method by studying the maximum echo amplitude of even harmonics as a function of pulse separation T. Note the possibility of a different functional dependence on T for even and odd harmonics.

(B) - In the second collision model, valid generally for rotational and some vibrational transitions, collisions are assumed to be velocity-changing in their effect on coherences¹⁸. In this model, the elastic scattering amplitudes are identical for levels 1 and 2; a state independent collision interaction can lead only to velocity-changes (no instantaneous phase changes) associated with level coherences. Collisions affect populations and coherences in the same manner in this model, resulting in a maximum echo amplitude depending on an average of

of studying small velocity changes is also present in time resolved saturation spectroscopy^{1,4} but the signal is then an intricate mixture of contributions from both coherences and level populations. An alternative method for studying the effects of velocity-changing collisions on level populations using stimulated photon echoes has recently been reported.²⁰

One of us (J L C) is grateful to New York University for welcoming him for a stay during which this work was prepared. Support was received from the U.S. Office of Naval Research and the New York University Challenge Fund.

Appendix A.

Solution of the equations of motion.

The first step is to solve the non stationary equations of motion in the presence of a permanent standing-wave field. We seek a solution to describe the evolution of the system within a short time τ after the field has been switched on assuming the following conditions

$$|\Delta| \tau \ll 1, \quad Y_{ij} \tau \ll 1.$$

Starting with Eq. (1), and using the new variables :

$$\bar{P}_{12} = P_{12} e^{i\omega t}$$

$$D = \bar{P}_{12} - \bar{P}_{21}, \quad S = \bar{P}_{12} + \bar{P}_{21}, \quad Y = P_{22} - P_{11}, \quad \text{we obtain}$$

the set of equations :

$$(A1) \quad \begin{cases} \dot{N} + \gamma \frac{\partial}{\partial z} N = 2i Y D \sin kz \\ \dot{D} + \gamma \frac{\partial}{\partial z} D = 2i X N \sin kz \\ \dot{S} + \gamma \frac{\partial}{\partial z} S = 0 \end{cases} \quad (A2)$$

The spatial derivative is eliminated by substitution using Fourier-series developments for the variables N, D, S .

$$(A3) \quad \begin{cases} \dot{N}_n + i n k v N_n = X (D_{n-1} - D_{n+1}) \\ \dot{D}_n + i n k v D_n = X (N_{n-1} - N_{n+1}) \\ \dot{S}_n + i n k v S_n = 0 \end{cases}$$

where the Fourier components are defined by :

$$(A4) \quad A = \sum_{n=-\infty}^{\infty} A_n e^{inikz}, \quad A = D, S, N.$$

At $t = t_0$, $D_0 = 0$ and $N_0 \neq 0$. It then follows from Eqs. (A3), that N_n is non zero for even n only and D_n is non zero for odd n only. Consequently, the two first equations of (A3) may be written in the form :

$$(A5) \quad \dot{Y}_n + i n k v Y_n = X (Y_{n-1} - Y_{n+1})$$

where $Y_n = N_n$ for even n and $Y_n = D_n$ for odd n .

The Y_n may be regarded as the components of a vector Y which can be expanded on a basis of eigenvectors of Eqs. A5. The components x_n of an eigenvector X associated with the eigenvalue λ_1 satisfy :

$$\dot{x}_n = \lambda_1 x_n.$$

and we obtain the system of linear equations :

$$(A6) \quad (\lambda + i n k v) x_n = X (x_{n-1} - x_{n+1})$$

Equations A6 may be solved by a method analogous to that used by Foldman and Feld²¹. One sets :

$$(A7) \quad x_n = (-i)^n c_n(\zeta)$$

with $v = n-1 \lambda/kv_z$ and $\zeta = 2x/kv_z$, which transforms Eqs. (A6) into:

$$(A8) \quad C_{v+1} + C_{v-1} = \frac{2v}{\zeta} C_v$$

The general solution of this system is:

$$(A9) \quad C_v(\zeta) = A J_v(\zeta) + B J_{-v}(\zeta)$$

where the J_v 's are Bessel functions. In terms of the initial variables we obtain:

$$x_n = (-1)^n \left[A(\lambda, \lambda, kv_z, t) J_{n-1} \lambda/kv_z \left(\frac{2x}{kv_z} \right) + B(\lambda, \lambda, kv_z, t) J_{-n+1} \lambda/kv_z \left(\frac{2x}{kv_z} \right) \right]$$

As there is no damping in the initial equations, we retain only the purely imaginary eigenvalues in (A6). An even more restrictive condition on the eigenvalues is placed by requiring $x_n \rightarrow 0$ as $n \rightarrow \infty$ for convergence of the series (A4). Since $J_v(z)$ diverges when $n \rightarrow \infty$ and v is not an integer, we keep λ such that $i \lambda/kv_z$ is an integer. Thus the general solution for $y_n(t)$ given as a linear combination of the $x_n(t)$ is:

$$(A10) \quad y_n(t) = (-1)^n \sum_{p=-\infty}^{+\infty} a_p(\lambda, kv_z) J_{n+p} \left(\frac{2x}{kv_z} \right) e^{ipkv_z(t-t_0)}$$

In order to express $y_n(t)$ in terms of initial conditions, Eq. (A10) is inverted at $t=t_0$, using the closure relation of Bessel functions²²:

$$(A11) \quad \sum_{m=-\infty}^{+\infty} J_m(x) J_m(x) = \delta_{m-m'}$$

to obtain

$$(A12) \quad a_p(\lambda, kv_z) = \sum_m J_{m+p} \left(\frac{2x}{kv_z} \right) y_m(t_0) (-1)^m$$

Substituting Eq. (A12) into (A10) and using the summation formula for Bessel functions²²:

$$(A13) \quad e^{im \left(\frac{x}{z} - \frac{t}{c} \right)} J_m \left(2z \sin \frac{\theta}{2} \right) = \sum_{s=-m}^{+\infty} J_s(x) J_{s+m}(x) e^{is\theta}$$

we finally obtain:

$$(A14) \quad y_n(t) = \sum_m y_m(t_0) e^{-i(n+m) \frac{kv_z}{2}(t-t_0)} \times J_{n-m} \left(\frac{4x}{kv_z} \sin \frac{kv_z(t-t_0)}{2} \right)$$

This solution is equivalent to that obtained in Appendix B by directly integrating Eqs. (A2). One notes that the n^{th} harmonic is driven by all m^{th} harmonics present at t_0 .

This result enables us to calculate the polarization of the gas sample after a sequence of two square pulses. At t_0 , the only non-zero spatial component is $N_0 = y_0$. The external field is on until $t_0 + \tau_0$. At this time the atomic spatial components are

$$\begin{cases} y_n(t_0 + \tau_0) = N_0(t_0) e^{-in \frac{kv_z \tau_0}{2}} J_n \left(\frac{4x}{kv_z} \sin \frac{kv_z \tau_0}{2} \right) \\ S_n = 0 \end{cases}$$

Following the pulse, the atoms evolve freely, and obey the equations:

$$(A15) \quad \begin{cases} \dot{N}_n + in kv_z N_n + \gamma N_n = 0 \\ \dot{D}_n + in kv_z D_n + \gamma_{12} D_n = i(\omega - \omega_0) S_n \\ \dot{S}_n + in kv_z S_n + \gamma_{12} S_n = i(\omega - \omega_0) D_n \end{cases}$$

where, for sake of simplicity, we have assumed that $\gamma_{11} = \gamma_{22} = \gamma$. At time t_1 , the solutions are:

$$N_n(t_1) = N_n(t_0 + \tau_0) e^{-\gamma(t_1 - t_0)} - \text{in } kv_z(t_1 - t_0)$$

$$(A16) \quad D_n(t_1) = D_n(t_0 + \tau_0) \cos(\omega - \omega_0)(t_1 - t_0) e^{-\text{in } kv_z(t_1 - t_0)} - \gamma_{12}(t_1 - t_0)$$

$$S_n(t_1) = i D_n(t_0 + \tau_0) \sin(\omega - \omega_0)(t_1 - t_0) e^{-\text{in } kv_z(t_1 - t_0)} - \gamma_{12}(t_1 - t_0)$$

The field is switched on from t_1 to $t_1 + \tau_1$, and $y_n(t_1 + \tau_1)$ can

be determined from Eq. (A14) using initial conditions (A16). Following

this pulse the system evolves freely until time t according to Eqs. (A15).

At time t one must calculate:

$$(A17) \quad \bar{P}(v_z, z, t) = 2 \frac{k}{x} \int_0^x P(v_z, z', t) \sin k(z' - z) dz.$$

$$(A18) \quad \text{where } P(v_z, z, t) = \mu(\rho_{12} + \rho_{21}) = \mu(S \cos \omega t - i D \sin \omega t).$$

Substituting (A18) into (A17) and using the Fourier expansions of

D and S , one finds:

$$(A19) \quad \bar{P}(v_z, z, t) = \bar{P}_c(v_z, z, t) \cos \omega t + \bar{P}_s(v_z, z, t) \sin \omega t$$

$$\text{where } \bar{P}_c(v_z, z, t) = i \mu(S_{-1} S_{-1}) \quad \text{and} \quad \bar{P}_s(v_z, z, t) = \mu(D_{-1} D_{-1}).$$

The quantities $S_{\pm 1}, D_{\pm 1}$ calculated by the procedure above are:

$$D_{\pm 1} = N_0 \cos(\Delta(t - t_1)) (A_{\pm} \cos \Delta \tau e^{-\gamma_{12} \tau} + B_{\pm} e^{-\gamma \tau})$$

$$(A20) \quad S_{\pm 1} = i N_0 \sin(\Delta(t - t_1)) (A_{\pm} \cos \Delta \tau e^{-\gamma_{12} \tau} + B_{\pm} e^{-\gamma \tau})$$

where:

$$A_{\pm} = \sum_{\text{odd } n} (-1)^{n+1} J_{n\pm 1} \left(\frac{4x}{kv_z} \sin \frac{kv_z \tau}{2} \right) J_n \left(\frac{4x}{kv_z} \sin \frac{kv_z \tau_0}{2} \right)$$

$$(A21) \quad B_{\pm} = \sum_{\text{even } n} \dots$$

$$\times \exp\left(-i kv_z [n \tau \pm (t - t_1) - \frac{n}{2} (\tau_0 - \tau_1) \pm \frac{\tau_1}{2}] - \gamma_{12}(t - t_1)\right).$$

Using the symmetry properties of the Bessel functions one finds the echo amplitude

$$(A22) \quad \mathcal{E}(z, t) = 2\pi k_f \int dv_z \left[\bar{P}_c(v_z, z, t)^2 + \bar{P}_s(v_z, z, t)^2 \right]^{1/2} \\ = 4\pi k_f \int dv_z \left[A \cos(\Delta \tau)_0 e^{-\gamma_{12} \tau} + B e^{-\gamma \tau} \right]$$

where

$$(A23) \quad A = \sum_{\text{odd } n} (-1)^n J_{n+1} \left(\frac{4x}{kv_z} \sin \frac{kv_z \tau}{2} \right) \times J_n \left(\frac{4x}{kv_z} \sin \frac{kv_z \tau_0}{2} \right) \\ B = \sum_{\text{even } n} \dots$$

$$\times \cos \left[kv_z \left(\mu \left(\tau - \frac{\tau_0 - \tau_1}{2} \right) - (t - t_1 + \frac{\tau_1}{2}) \right) \right] \times \exp - \gamma_{12}(t - t_1).$$

Appendix B.

In Appendix A we have solved the equations in a manner which exhibits the successive echoes which are associated with the Fourier components of the solution. The equations may also be solved directly to exhibit the motion of a group of atoms starting at (v_z, z_0, t_0) .

Adding the two first equations in (A2) term to term we obtain:

$$(B1) \quad \dot{y} + v_z \frac{\partial y}{\partial z} = 2i x y \sin kz$$

$$(B2) \quad \text{where } y = N + D.$$

Changing variables (z, t) to $(x = z - v_z t, t)$ one gets:

$$(B3) \quad \frac{\partial y}{\partial t} = 2i x y \sin k(x + v_z t).$$

The integration leads to :

$$(24) \quad y(x, t) = y(x_0, t_0) \exp(2iX) \int_{t_0}^t \sin k(x + v_x t') dt'$$

where :

$$z = z_0 - v_x t = z_0 - v_x t_0$$

With a boundary value condition at (z_0, t_0) , one obtains :

$$(25) \quad y(z_0 + v(t-t_0), t) = y(z_0, t_0) \exp(2iX) \int_{t_0}^t \sin k(z_0 + v(t'-t_0)) dt'$$

As an atom experiences the field $\chi(z_0, t'-t_0) = X \sin k(z_0 + v(t'-t_0))$

at time t' , the integral in (25) can be understood as an average over the field amplitude along the atomic path during the pulse.

Thus :

$$\langle \chi(z_0, t'-t_0) \rangle_{z_0-t} = X \int_{t_0}^t \sin k(z_0 + v(t'-t_0)) dt'$$

and :

$$\begin{aligned} X(z_0 + v(t-t_0), t_0) &= X(z_0, t_0) \cos[2(t-t_0) \langle \chi(z_0, t'-t_0) \rangle] \\ &\quad - X(z_0, t_0) \sin[2(t-t_0) \langle \chi(z_0, t'-t_0) \rangle] \\ Y(z_0 + v(t-t_0), t_0) &= Y(z_0, t_0) \cos[2(t-t_0) \langle \chi(z_0, t'-t_0) \rangle] \\ &\quad + X(z_0, t_0) \sin[2(t-t_0) \langle \chi(z_0, t'-t_0) \rangle] \end{aligned}$$

References.

- 1 T. W. Hünsch, I. S. Shahin, A. L. Shawlow, Phys. Rev. Lett. **27**, 707 (1971).
- Ph. Cahuzac, X. Drago, Optics Commun. **24**, 63 (1978).
- 2 R. G. Brewer, R. L. Shoemaker, Phys. Rev. **6**, 2001 (1972).
- 3 J. P. Gordon, C. H. Wang, C. K. N. Patel, R. E. Slusher, W. J. Tomlinson, Phys. Rev. **179**, 294 (1969).
- 4 P. R. Berman, J. M. Levy, R. G. Brewer, Phys. Rev. A **11**, 1668 (1975).
- 5 S. Harocho, J. A. Paisner, A. L. Shawlow, Phys. Rev. Lett. **32**, 948 (1973).
- 6 J. R. R. Leite, R. L. Sheffield, M. Dudley, R. D. Sharma, M. S. Feld, Phys. Rev. A **14**, 1151 (1976).
- 7 J. C. Mac Gillivray and M. S. Feld, Phys. Rev. A **14**, 1169 (1976).
- 8 Ye. V. Baklanov, V. P. Chebotayev, B. Ya. Dubetsky, Appl. Phys. **11**, 201 (1976).
- 9 J. C. Borquist, S. A. Lee, J. L. Hall, Phys. Rev. Lett. **32**, 159 (1977).
- 10 V. P. Chebotayev, A. V. Shishayev, B. Ya. Yarshin, I. S. Vasilenko, Appl. Phys. **15**, 43 (1978).
- 11 S. N. Bagayev, V. P. Chebotayev, A. S. Dychkov, Appl. Phys. **15**, 209 (1978).
- V. P. Chebotayev, Appl. Phys. **15**, 219 (1978).
- 12 M. M. Salour, C. Cohen-Tannoudji, Phys. Rev. Lett. **14**, 757 (1977).
- 13 V. P. Chebotayev, N. M. Dyaba, M. I. Skvorstov, I. S. Vasilenko, Appl. Phys. **15**, 319 (1978).
- 14 The values for $n=1$ are close to those required to maximize the classical photon echo : $2X \tau_0 = \pi/2$, $2X \tau_1 = \pi$.
- 15 S. N. Bagayev, E. V. Baklanov, V. I. Chebotayev, Pis'ma Red. Zh. Teor. Fiz. **16**, 15 (1972) ; **16**, 344 (1972) [Sov. Phys. J.E.T.P. Lett. **16**, 9

(1972) ; 16, 243 (1972) ;

Y. V. Smith, T. W. Hensch, Phys. Rev. Lett. 26, 740 (1971) ;

C. Bréchinac, R. Vetter, P. R. Berman, J. Phys. B 10, 3443 (1977) ;
Phys. Rev. A 17, 1609 (1978) ;

J. L. Le Gouët, J. Phys. B 11, 3001 (1978).

¹⁶ Unequal decay rates are treated by A. Schenzle and R. G. Brewer, Phys. Rev. A 14, 1756 (1976).

¹⁷ Longer pulses lead to a modification of the maximum echo amplitude through Eq. (9) and to the possibility that collisions can remove atoms from the limited velocity classes excited by a long pulse. The collisional effect can be compensated for by an appropriate increase in Γ_1 .

¹⁸ P. R. Berman, Appl. Phys. (Germany) 6, 283 (1975).

¹⁹ For weak velocity-changing collisions $\alpha = \frac{1}{2}$. (Note: Δu in Ref. 4

$= \sqrt{2} \Delta u$) of this work). For weak collisions, an expression for the entire range of $k\Delta u t$ (see Ref. 4 and A. Flusberg, to appear in Opt. Comm.) may be obtained. Expressions of the form $\langle \exp(\int_{t_1}^{t_2} k v_2 dt) \rangle$ lead to an echo contribution going as

$$\exp \left\{ - \int_0^{t_1} (\Gamma - \int V(v-v') \exp[ink(v-v')t] dv') dt \right\}$$

where $V(v-v')$ is the collision kernel. This equation provides the limits shown in Eqs. (13) and (14).

²⁰ T. Mossberg, A. Flusberg, R. Kachru, and S.R. Hartmann, Bull. Am. Phys. Soc. 24, 25 (1979).

²¹ B.J. Feldmann, M.S. Feld, Phys. Rev. A1, 1375 (1970).

²² I.S. Gredshcheyn, I.M. Ryzhik, Table of integrals series and products, Academic Press (1965).

Figure captions.

Figure 1 : Two standing wave pulses of duration τ_0 and τ_1 separated by time T are incident on an atomic system.

Figure 2 : Schematic representation of the results : (a) Input pulses, (b) output as a function of time, (c) output as a function of detuning for fixed t located at one of the echoes occurring at $t = \tau_1 + nT$ with n odd.

Figure 3 : Maximum value of the first echo amplitude as a function of $k u \tau_1$ for various ratios $\chi/k u$. The value of τ_0 was taken equal to $0.58\tau_1$.

Figure 4 : Maximum value of the second echo amplitude as a function of $k u \tau_1$ for various ratios $\chi/k u$. The value of τ_0 was taken equal to $0.74\tau_1$.

Figure 5 : First echo amplitude ($n=1$) as a function of time for various field strengths $\chi/k u$. The values of $k u \tau_1$ used to minimize the amplitude are indicated on the figure.

Figure 6 : Second echo amplitude ($n=2$) as a function of time for various field strengths $\chi/k u$.

Figure 7 : Evolution of the spatial phase of the (-1) harmonic as a function of time, showing only the contribution from the 8th harmonic following the second pulse. This contribution leads to an echo at $t = \tau_1 + 8T$. Contributions from other harmonics (not shown) lead to echoes at $t = \tau_1 + |n| T$.

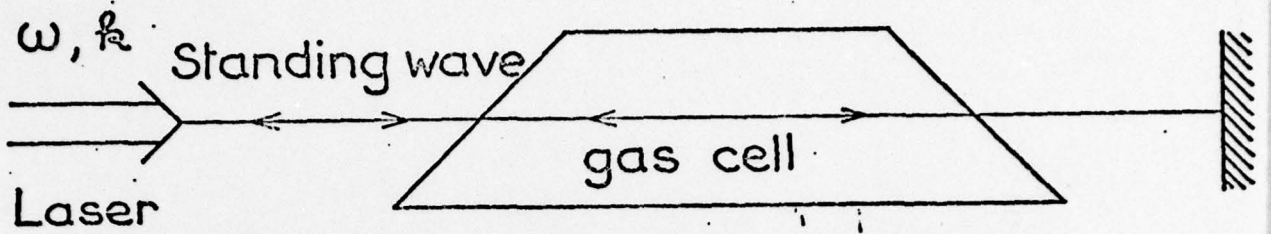


Fig. 1

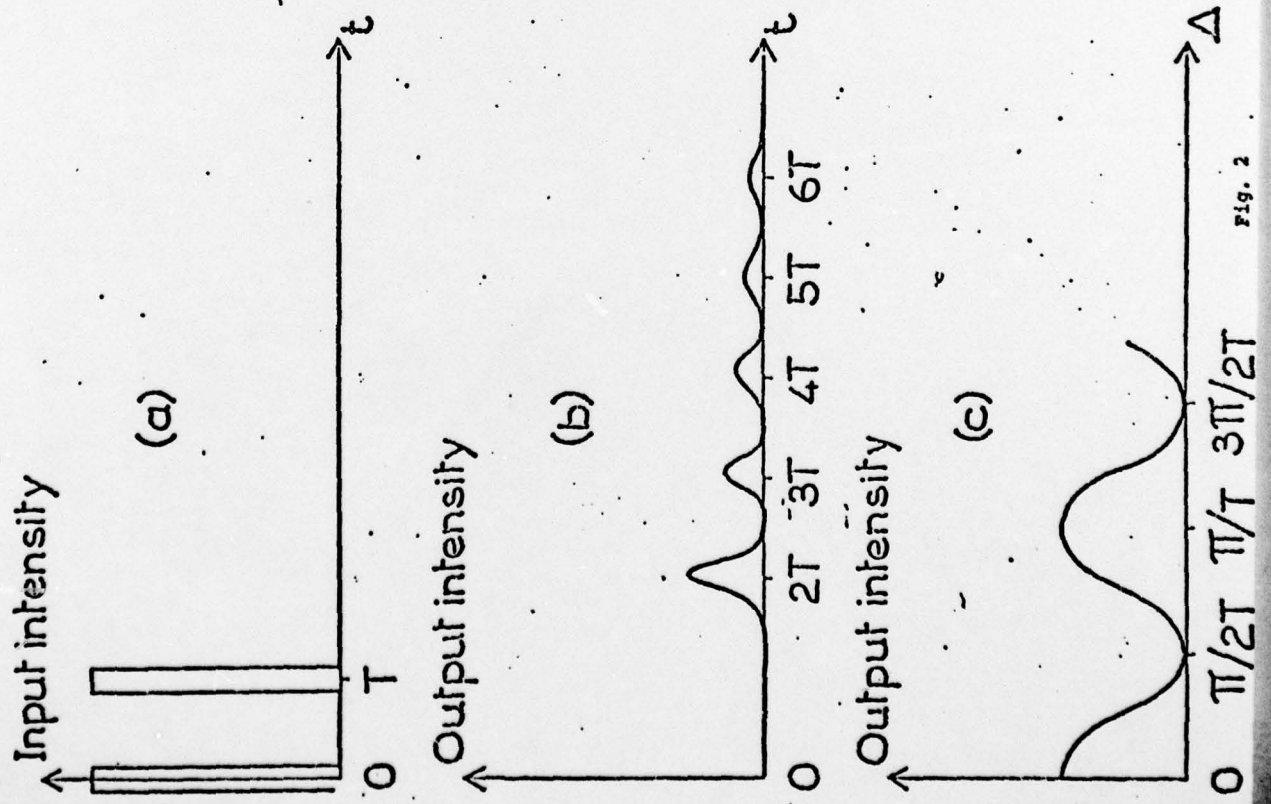
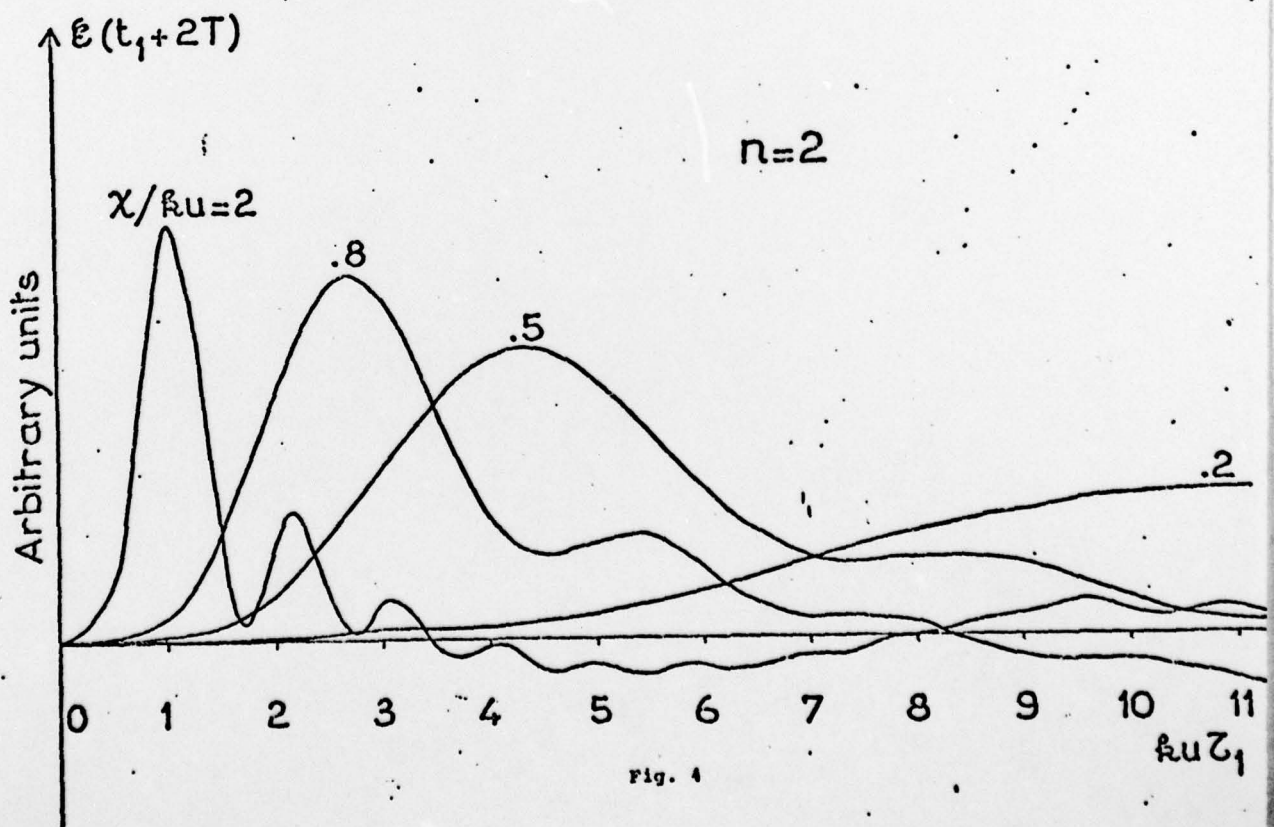
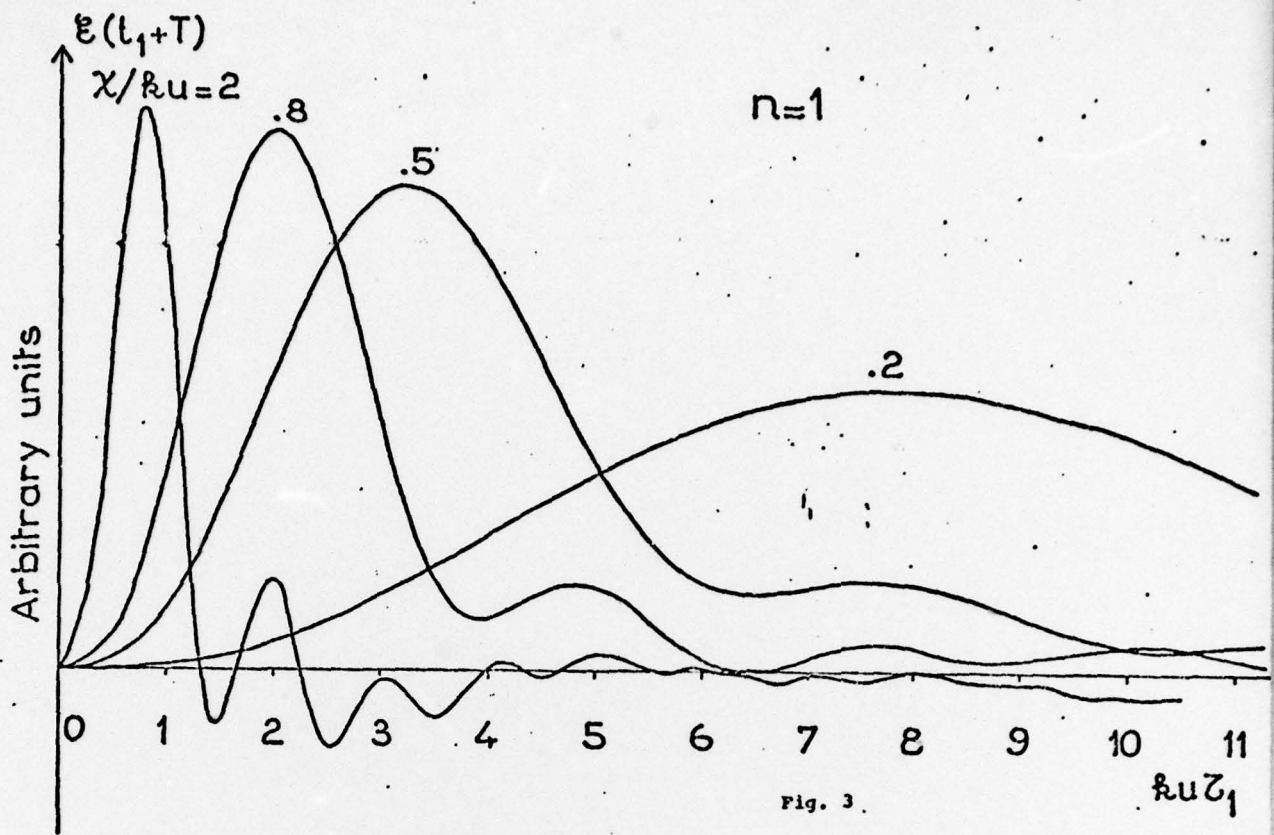
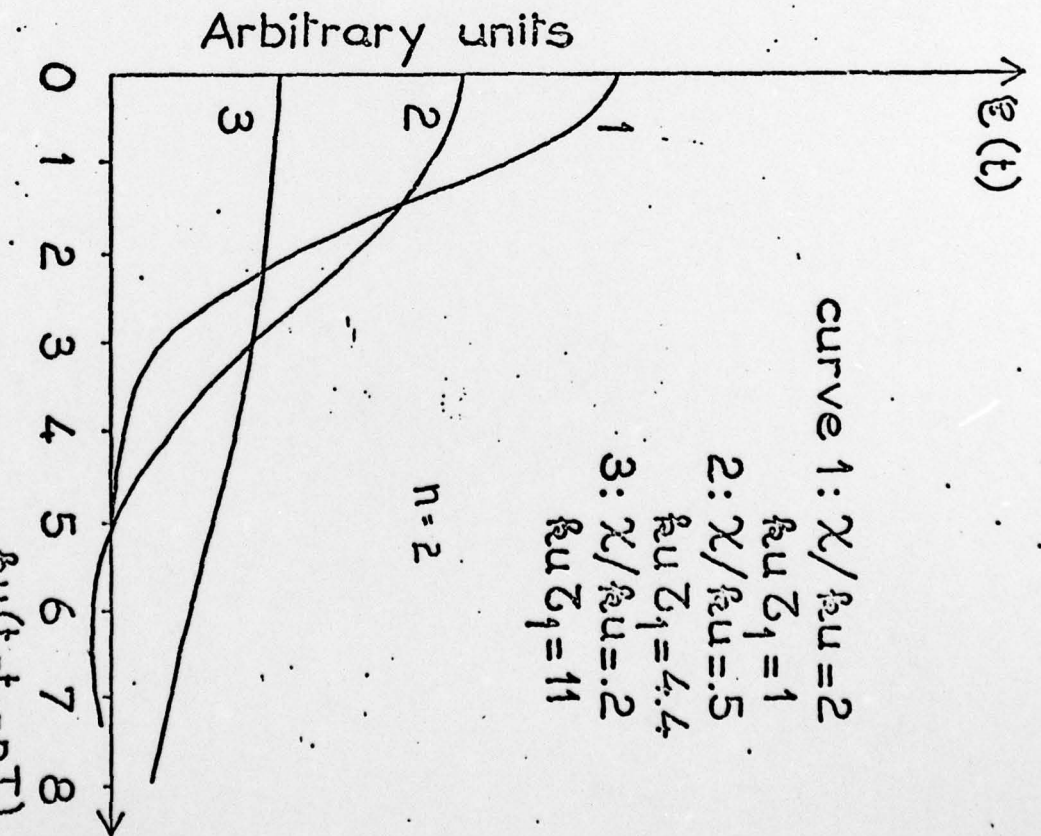
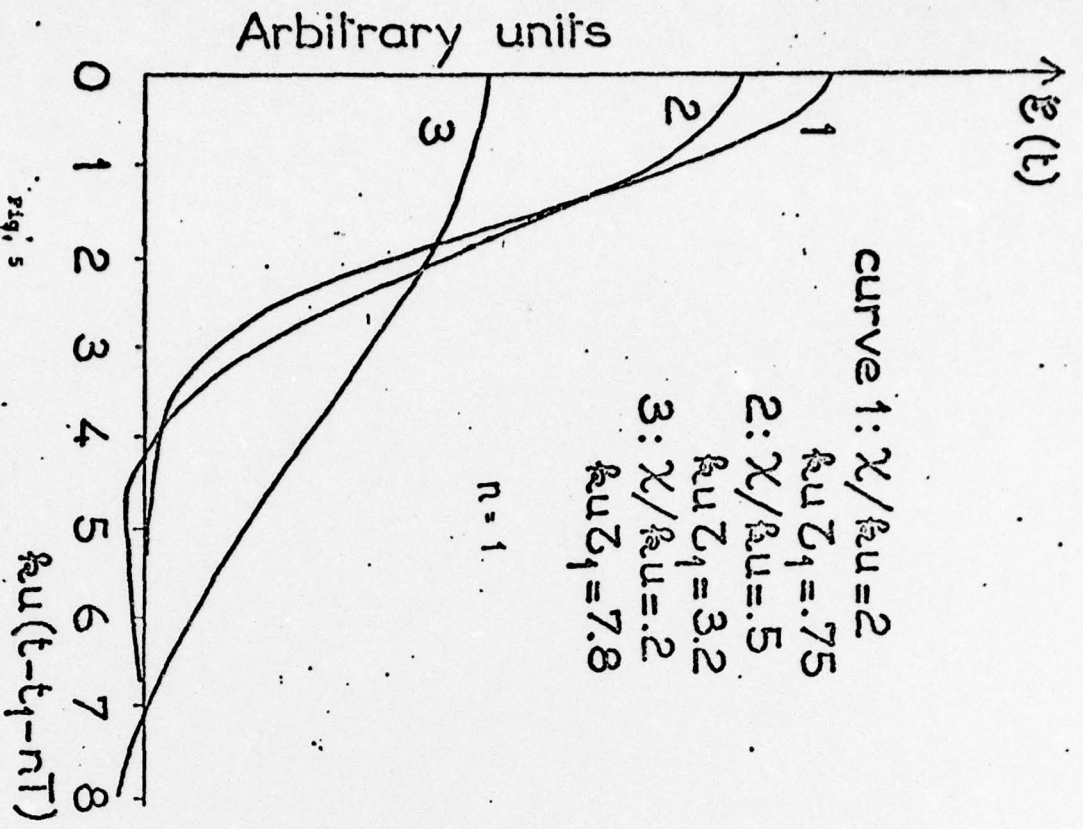


Fig. 2





F. 5

Fig. 5

F. 6

Fig. 6

$\varphi_{n+1}(v_z, z, t)$

$m=1$
 $n=+8$
 $z=0$

$\delta v_z(t_1 - t_0)$

$t_1 + |n|T$
 t

$-\delta v_z(t_1 - t_0)$

Fig. 7